RAA 2019 Vol. **19** No. **8**, 118(8pp) doi: 10.1088/1674–4527/19/8/118

http://www.raa-journal.org *http://iopscience.iop.org/raa*

***R**esearch in*
***A**stronomy and*
***A**strophysics*

Revisiting the event rate of short GRBs and estimating their detectable number within the Advanced LIGO horizon

Hao-Yang Liu and Yun-Wei Yu

Institute of Astrophysics, Central China Normal University, Wuhan 430079, China; *yuyw@mail.ccnu.edu.cn*

Received 2018 December 21; accepted 2019 March 26

Abstract The redshift and luminosity distributions of 36 *Swift* short gamma-ray bursts (GRBs) are fitted by connecting their event rates with cosmic star formation rates using power-law distributed delay times $f(\tau) \propto \tau^{-1}$, where a broken-power-law luminosity function is assumed and some empirical observational selection effects are taken into account. As a result, the most-likely model parameters are constrained to be $\nu_1 = 0.91$, $\nu_2 = 1.66$ as power-law indices, with a break at $L_b = 2.51 \times 10^{51}\,\mathrm{erg\,s^{-1}}$ for the luminosity function and $\tau_c = 6.0\,\mathrm{Gyr}$ for a typical gravitational wave decay timescale of the binary orbit. The corresponding local rate of short GRBs is found to be $\sim (3-4)\,\mathrm{Gpc^{-3}\,yr^{-1}}$. With these parameters, the detectable numbers of short GRBs are estimated within the horizon of Advanced LIGO.

Key words: gamma-ray burst: general — luminosity function — stars: neutron

1 INTRODUCTION

Gamma-ray bursts (GRBs) are usually divided into two classes by a separating line at $T_{90} = 2\,\mathrm{s}$ (Kouveliotou et al. 1993), where T_{90} is the time interval observed to contain 90 percent of the prompt emission. On one hand, long-duration GRBs with $T_{90} > 2\,\mathrm{s}$ are believed to originate from the collapses of massive stars, which have been demonstrated by their association with Type Ib/c supernovae (Stanek et al. 2003; Hjorth et al. 2003; Chornock et al. 2010). Therefore, the event rates of long GRBs are usually used as a tracer to probe cosmic star formation rates (CSFRs). On the other hand, it has long been hypothesized that short-duration GRBs could be produced by mergers of compact binaries, i.e., neutron star-neutron star (NS-NS) or neutron star-black hole (NS-BH) binaries (Paczynski 1986; Eichler et al. 1989; Narayan et al. 1992). This hypothesis was strongly supported by the non-detection of supernovae associated with short GRBs and by the relatively large offsets of short GRBs from their host galaxies. Eventually, on 2017 August 17, a gravitational wave (GW) signal coming from a merger of double NSs (i.e., GW170817) was detected by LIGO/Virgo for the first time in history, which was followed by a short GRB (i.e., GRB 170817A) with a 1.7-second lag (Abbott et al. 2017; Goldstein et al. 2017). The GW170817-GRB 170817A association definitely confirmed that some short GRBs arise from mergers of compact binaries.

The event rate of GW170817-like NS-NS mergers could be as high as $1540^{+3200}_{-1220}\,\mathrm{Gpc^{-3}\,yr^{-1}}$ (Abbott et al. 2017; Zhang et al. 2018), which was estimated from the horizon and period of the search by LIGO during O2. This value is significantly higher than the previous estimates for short GRBs that range from a few to a few tens per cubic giga-parsec per year (Guetta & Piran 2006; Nakar et al. 2006; Guetta & Stella 2009; Dietz 2011; Coward et al. 2012; Wanderman & Piran 2015; Tan et al. 2018). Specifically, in previous statistical studies of short GRBs, an event rate of around $\dot{R}_{\mathrm{sGRB}}(0) \approx 4\ \mathrm{Gpc^{-3}\,yr^{-1}}$ was widely accepted for an assumed minimum luminosity of $L_{\min} \sim 5 \times 10^{49}\,\mathrm{erg\,s^{-1}}$. The discrepancy between the short GRB rate and the NS-NS merger rate could primarily arise from the high collimation of GRB jets. By introducing a half-opening angle θ_{j} of the jets, the ratio $1-\cos\theta_{\mathrm{j}} \sim 4/1540$ could lead to $\theta_{\mathrm{j}} \sim 4^{\circ}$, which is broadly consistent with some previous measurements (Fong et al. 2015; Jin et al. 2018).

However, the discovery of GRB 170817A, which indicates a short GRB rate of $> 190^{+440}_{-160}\,\mathrm{Gpc^{-3}\,yr^{-1}}$ (Zhang et al. 2018), could still challenge the above understanding if the same beaming angle is assumed. In any case,

one fact that should be noticed is that the observation of GRB 170817A is obviously off-axis, which is implied by the absence of its early afterglow emission and also indicated by the GW detection. The viewing angle can be constrained to $> 30^\circ$. Meanwhile, the isotropically-equivalent luminosity of GRB 170817A was found to be on the order of $10^{47}\,\mathrm{erg\,s^{-1}}$, which is much lower than the usually-adopted minimum luminosity for short GRBs. These properties may indicate that GRB 170817A belongs to a completely new type of GRB with a large-angle jet and an intrinsically low luminosity, if the jet is uniform. In this case, it may be indicated that the opening angles of GRB jets are anti-correlated with their luminosities. The lower the luminosity, the larger the opening angle. Nevertheless, as another possibility, the low luminosity of GRB 170817A could just correspond to an emission from the edge of a structured GRB jet, while the emission from the core of the jet is still as bright as that of normal short GRBs. By considering an opening angle of the jet core $\sim 4^\circ$, the ratio between the rates of $\sim 4\,\mathrm{Gpc^{-3}\,yr^{-1}}$ and $\sim 190\,\mathrm{Gpc^{-3}\,yr^{-1}}$ can naturally be accounted for by the ratio $(1-\cos 4^\circ)/(1-\cos 30^\circ)$. More importantly, recent studies on the late multi-wavelength afterglows of GRB 170817A have strongly favored this off-axis structured jet model (Gill & Granot 2018; Lazzati et al. 2018; Mooley et al. 2018), which will therefore be considered in this paper.

In the framework of the structured jet model, the so-called normal short GRBs are generally observed on-axis and their minimum isotropically-equivalent luminosity could be around several times $10^{49}\,\mathrm{erg\,s^{-1}}$. For any short GRB, its luminosity could decrease rapidly with an increasing viewing angle relative to its symmetry axis and thus it can be observed off-axis only if its distance is small enough. Therefore, in order to estimate the future GW-GRB association rate more exactly, it is necessary to revisit the connection between the event rate of on-axis short GRBs and the rate of NS-involved mergers, and then to take into account the influence of the angular distribution of jet properties.

2 THE MODEL

2.1 The Rate of Short GRBs

Because of the merger origin of short GRBs, where all short GRBs used here are assumed to be physically related to merger events, their event rate at redshift z can in principle be determined by the CSFR at redshift z'. Here the redshifts z and z' are connected by a delay time τ that is due to the formation of the compact binary and the gravitational radiation decay of the binary orbit, i.e., $t(z') = t(z) - \tau$, where $t(z) = \int_z^\infty [(1+z')H(z')]^{-1}dz'$ is the age of the universe at redshift z and $H(z) \equiv H_0\sqrt{\Omega_{\rm M}(1+z)^3+\Omega_\Lambda}$. Throughout this paper, the cosmological parameters are taken as $\Omega_M = 0.32, \Omega_\Lambda = 0.68$ and $H_0 = 70\,\mathrm{km\,s^{-1}\,Mpc^{-1}}$. Then, by invoking a probability distribution for the delay time $P(\tau)$, we can calculate the rate of short GRBs by the following convolution (Piran 1992; Guetta & Piran 2006)

$$\begin{aligned}\dot{R}_{\rm SGRB}(z) &\propto \int_0^{t(z)-t(z_{\rm b})} \dot{\rho}_*[t(z)-\tau]P(\tau)d\tau \\ &\propto \int_z^{z_{\rm b}} \dot{\rho}_*(z')P[t(z)-t(z')]\frac{dt}{dz'}dz', \quad (1)\end{aligned}$$

where $\dot{\rho}_*(z)$ is the CSFR and $dt/dz = -[(1+z)H(z)]^{-1}$. The upper limit of the integration, $z_{\rm b}$, is set at the redshift when compact binaries started forming.

It is not easy to give a precise but simple expression for the probability function $P(\tau)$, because of the complexity inherent in the delay time. While the formation time of a compact binary is determined by the supernova mechanism, natal kick velocity of NSs, mass transfer between binary stars, etc (Portegies Zwart & Yungelson 1998; Belczynski et al. 2002; Mennekens et al. 2010; Chruslinska et al. 2018), the gravitational radiation timescale is sensitive to the initial orbital separation (a_i) and initial ellipticity (e_i). In this paper, we will take an empirical function as (Cao et al. 2018)

$$P(\tau) \propto \left(\frac{\tau}{\tau_{\rm c}}\right)^{-1} e^{-\tau_{\rm c}/\tau}, \quad (2)$$

which can be understood as GW radiation with power-law distributed orbital separations and a constant ellipticity. On one hand, this delay time distribution has been widely and successfully applied in modeling the redshift distribution of short GRBs (Guetta & Piran 2006; Nakar et al. 2006; Virgili et al. 2011; Hao & Yuan 2013; Wanderman & Piran 2015). Furthermore, this distribution has also been supported by the observational delay time distribution of type Ia supernovae that could mainly originate from mergers of double white dwarfs (Totani et al. 2008; Maoz et al. 2012). On the other hand, theoretically, elaborate simulations of compact binaries always gave rise to such a power-law delay time distribution (Greggio 2005; Belczynski et al. 2006; Mennekens et al. 2010; Ruiter et al. 2011; Mennekens & Vanbeveren 2016). In any case, the integrated result in Equation (1) is primarily dependent on the value of the crucial cutoff in delay times $\tau_{\rm c}$, which is probably around a few hundred Myr for double NS mergers, but

around a few tens of Myr for NS-BH mergers (Mennekens & Vanbeveren 2016; Chruslinska et al. 2018).

The cosmic star formation history is adopted as follows (Yu et al. 2012)

$$\dot{\rho}_*(z) \propto \begin{cases} (1+z)^{3.44}, & \text{for } z < 0.97, \\ (1+z)^{0}, & \text{for } 0.97 \leq z < 3.5, \\ (1+z)^{-0.8}, & \text{for } z \geq 3.5, \end{cases} \quad (3)$$

with a local CSFR of $\dot{\rho}_*(0) = 0.02\,M_\odot\,\mathrm{yr}^{-1}\,\mathrm{Mpc}^{-3}$. Here, while the CSFRs at relatively low redshifts have been basically fixed by a series of measurements of CSFRs (Hopkins & Beacom 2006), the decrease rate in CSFRs at high redshifts is still under debate. In Hopkins & Beacom's data, a trend of decreasing CSFRs appears in the higher redshift range. The index -0.8 used here is obtained by combining the constraints from Gunn-Peterson trough observations to quasars and from the Thomson scattering optical depth of cosmic microwave background photons (e.g., Yu et al. 2012; Wang 2013). In any case, the uncertainty of the high-redshift CSFRs would not significantly influence the rates of short GRBs.

2.2 Number Distributions

For given merger rates, we can calculate the cumulative number of observational short GRBs for redshifts less than z by

$$N_{\rm obs}(<z) = \frac{\Delta\Omega}{4\pi} T f_{\rm B} \int_0^z \int_{L_{\rm th}(z')}^{L_{\rm max}} \dot{R}_{\rm SGRB}(z') \times \Phi(L)\vartheta_z(P,z')\mathrm{d}L\frac{\mathrm{d}V(z')}{1+z'}, \quad (4)$$

or for luminosities less than L by

$$N_{\rm obs}(<L) = \frac{\Delta\Omega}{4\pi} T f_{\rm B} \int_{L_{\rm min}}^{L} \int_0^{z_{\rm th}(L)} \dot{R}_{\rm SGRB}(z) \times \Phi(L)\vartheta_z(P,z)\frac{dV(z)}{1+z}\mathrm{d}L, \quad (5)$$

where $\Delta\Omega$ is the field of view of a telescope, T is the observational period and $f_{\rm B} = (1-\cos\theta_{\rm j})$ is the beaming factor corresponding to an opening angle $\theta_{\rm j}$ of effectively top-hat jets. $L_{\rm th}$ is the observational threshold of the telescope, below which the trigger probability decreases drastically, and $\vartheta_z(P,z)$ is the probability for redshift measurements of short GRBs. The comoving volume element is defined by $\mathrm{d}V(z) = 4\pi D_{\rm c}(z)^2 c dz/H(z)$ with $D_{\rm c}(z) = c\int_0^z H(z')^{-1}dz'$. The integrals in Equations (4) and (5) are strongly related to the luminosity function $\Phi(L)$ of short GRBs, which is however very uncertain. Two empirical forms of luminosity function are usually adopted and compared in the literature, i.e., a single power law with an exponential cutoff or a broken power law (Siellez et al. 2014; Ghirlanda et al. 2015, 2016). In comparison, the broken-power-law form was usually more favored by observational distributions of GRBs than the single power law (e.g. Cao et al. 2011). Therefore, in this paper we take

$$\Phi(L) \propto \begin{cases} \left(\frac{L}{L_{\rm b}}\right)^{-\nu_1}, & L < L_{\rm b}, \\ \left(\frac{L}{L_{\rm b}}\right)^{-\nu_2}, & L \geq L_{\rm b}. \end{cases} \quad (6)$$

2.3 Threshold and Selections

It is impossible to derive a precise expression, from first principles, for the probabilities of GRB triggers and redshift measurements, which can only be obtained empirically from observations. By using the *Swift* long GRB samples, Cao et al. (2011) obtained some empirical expressions for these selection effects. To be specific, they found a threshold average flux of $P_{\rm th} = 5\times10^{-9}\,\mathrm{erg\,s^{-1}\,cm^{-2}}$, above which GRBs can always trigger the *Swift* Burst Alert Telescope (BAT) successfully. Therefore, the luminosity threshold can be determined by

$$L_{\rm th}(z) = 4\pi D_{\rm l}(z)^2 k(z) P_{\rm th}, \quad (7)$$

where the luminosity distance $D_{\rm l}(z) = (1+z)d_{\rm c}(z)$ and $k(z)$ is the k-correction factor converting the observed flux into a wide common energy band for different redshifts. The redshift-measurement probability of a GRB is in principle dependent on both its flux and redshift. By fitting the redshift and luminosity distributions of *Swift* long GRBs, Cao et al. (2011) found that the probability can be approximatively written as

$$\vartheta_z(P,z) = \zeta(P)\eta(z), \quad (8)$$

where

$$\zeta(P) = \min\left[0.27 + \frac{P}{2\times10^{-6}\,\mathrm{erg\,s^{-1}\,cm^{-2}}}, 1\right] \quad (9)$$

and

$$\eta(z) = \begin{cases} 1-\exp[-\frac{2\sigma^2}{(z-\mu)^2}], & \text{for } L < L_*, \\ 1, & \text{for } L > L_*, \end{cases} \quad (10)$$

where $\mu = 1.8$, $\sigma = 0.56$ and $L_* \sim 2\times10^{51}\,\mathrm{erg\,s^{-1}}$. On one hand, the brighter the GRBs are, the easier the discovery of their afterglows and host galaxies is. Therefore, as indicated by $\zeta(P)$, the probability increases as an increasing flux. On the other hand, the expression of $\eta(z)$ indicates that redshift measurements can be somewhat suppressed within the range $1.1 < z < 2.1$, for relatively dark

GRBs. The reason is that the strong observable emission or absorption lines are transferred outside of the typical interval of optical spectrometers (Fiore et al. 2007), which is usually called the redshift desert effect.

In principle, the above selection effects are primarily determined by the properties of telescopes and observational modes, but weakly dependent on GRB emissions. Therefore, it seems reasonable and convenient to adopt these selection effects for short GRBs, although they were obtained from long GRBs. After all, derivations of selection effects using short GRBs themselves are seriously hindered by their very limited number.

3 *SWIFT* SHORT GRBS AND PARAMETER CONSTRAINTS

The first discovery of the afterglow and host galaxy of a short GRB (i.e., GRB 050509B, Gehrels et al. 2005) was achieved in May 2015 by relying on the *Swift* X-Ray Telescope (XRT) and follow-up optical observations, which led to the measurement of its redshift. From then on, a total of 150 short GRBs was detected by *Swift*, out of which 36 were fixed by a redshift. The fraction of $36/150$ is consistent with the average value of the probability given by Equation (8). From the year 2008, the *Fermi* satellite started to join the hunt for GRBs and, up to now, has captured a total of 100 short GRBs. Nevertheless, in this paper we will only consider the short GRB samples provided by *Swift*, since the expressions of selection effects are all taken from Cao et al. (2011) which were obtained from *Swift* long GRBs. Furthermore, in order to concur with the adopted threshold, any GRBs with an average flux lower than $P_{\rm th}$ should be excluded if they exist. Then, the adopted short GRBs are listed in Table 1. Following Kistler et al. (2008, 2009) and Cao et al. (2011), the isotropically-equivalent energy release and average luminosity of a short GRB are given by

$$E_{\rm iso} = 4\pi D_{\rm c}^2(z) S k(z)(1+z) \tag{11}$$

and

$$L_{\rm iso} = \frac{E_{\rm iso}}{T_{90}/(1+z)}, \tag{12}$$

respectively, where S is the observed fluence. The k-correction factor is calculated using spectral indices $\alpha = -0.5$ and $\beta = -2.3$, and a typical peak energy $E_{\rm p} \sim 490\,{\rm keV}$ (Nava et al. 2011). The calculated $E_{\rm iso}$ and $L_{\rm iso}$ are listed in Table 1 and also scattered in the $z - L_{\rm iso}$ plane in Figure 1, where the *Swift* BAT threshold is represented by the solid line for comparison. The normalized cumulative distributions of the short GRBs in luminosity and redshift are presented in the left and right panels of Figure 2, respectively.

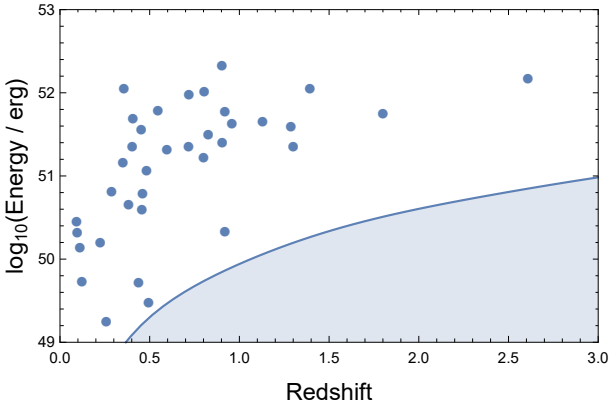

Fig. 1 Average luminosity vs. redshift of 36 *Swift* short GRBs. The *solid line* traces an effective threshold defined by *Swift* BAT corresponding to a flux threshold of $P_{\rm th} = 5 \times 10^{-9}\,{\rm erg\,s^{-1}\,cm^{-2}}$.

By varying the model parameters ν_1, ν_2, $L_{\rm b}$ and $\tau_{\rm c}$, we apply Equations (4) and (5) to fit the normalized redshift and luminosity distributions of the *Swift* short GRBs. The goodness of fit is assessed by the Kolmogorov-Smirnov test. As a result, constraints on the parameters from these fits are presented by the grey $1\sigma-$contours in Figure 3. The best fit can be obtained with parameters $\nu_1 = 0.91$, $\nu_2 = 1.66$, $L_{\rm b} = 2.51 \times 10^{51}\,{\rm erg\,s^{-1}}$ and $\tau_{\rm c} = 6.03\,{\rm Gyr}$. The corresponding fitting lines are displayed in Figure 2. Finally, in order to account for the absolute number of 36, the local rate of short GRBs can further be constrained, as signified by the dashed lines in Figure 3, which gives

$$R_{\rm SGRB,obs}(0) \sim (3-4)\,{\rm Gpc^{-3}\,yr^{-1}}, \tag{13}$$

where $\Delta\Omega/4\pi = 0.1$ and $T = 11\,{\rm yr}$ are taken. This result is basically consistent with previous studies. As discussed in the Introduction, the comparison of the above rate with the rate of $1540^{+3200}_{-1220}\,{\rm Gpc^{-3}\,yr^{-1}}$ inferred from the GW170817 observation indicates that the effective beaming factor of the assumed top-hat GRB jets is determined by an opening angle of around $3^\circ - 4^\circ$.

4 DETECTABLE RATE WITHIN THE ADVANCED LIGO HORIZON

In the above calculations, the GRB observations are all considered to be on-axis and the GRB jets have a top-hat structure. However, as mentioned in the Introduction, observations of GW170817 and GRB 170817A indicated that GRB jets probably have a wide angular distribution. To the lowest-order approximation, the energy distribution

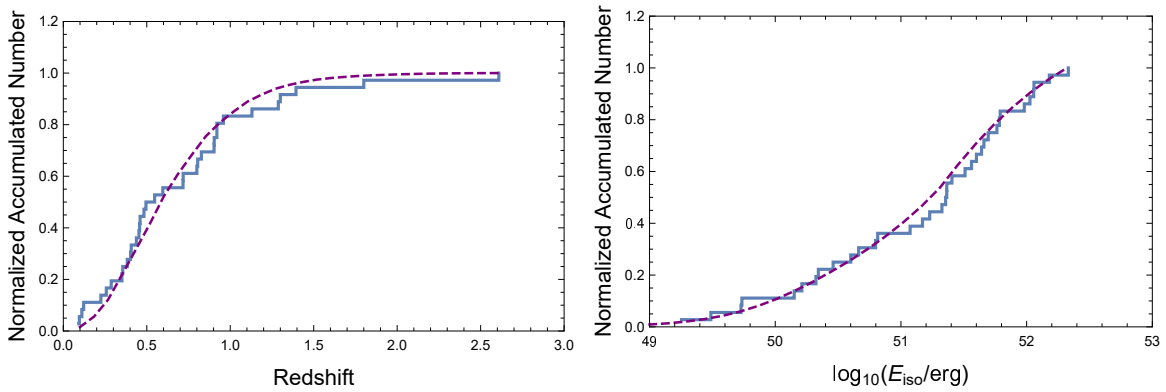

Fig. 2 Normalized cumulative distributions in luminosity (*left*) and redshift (*right*) for *Swift* short GRBs (*solid lines*). An example fitting to the distributions by the model is presented by the *dashed lines*.

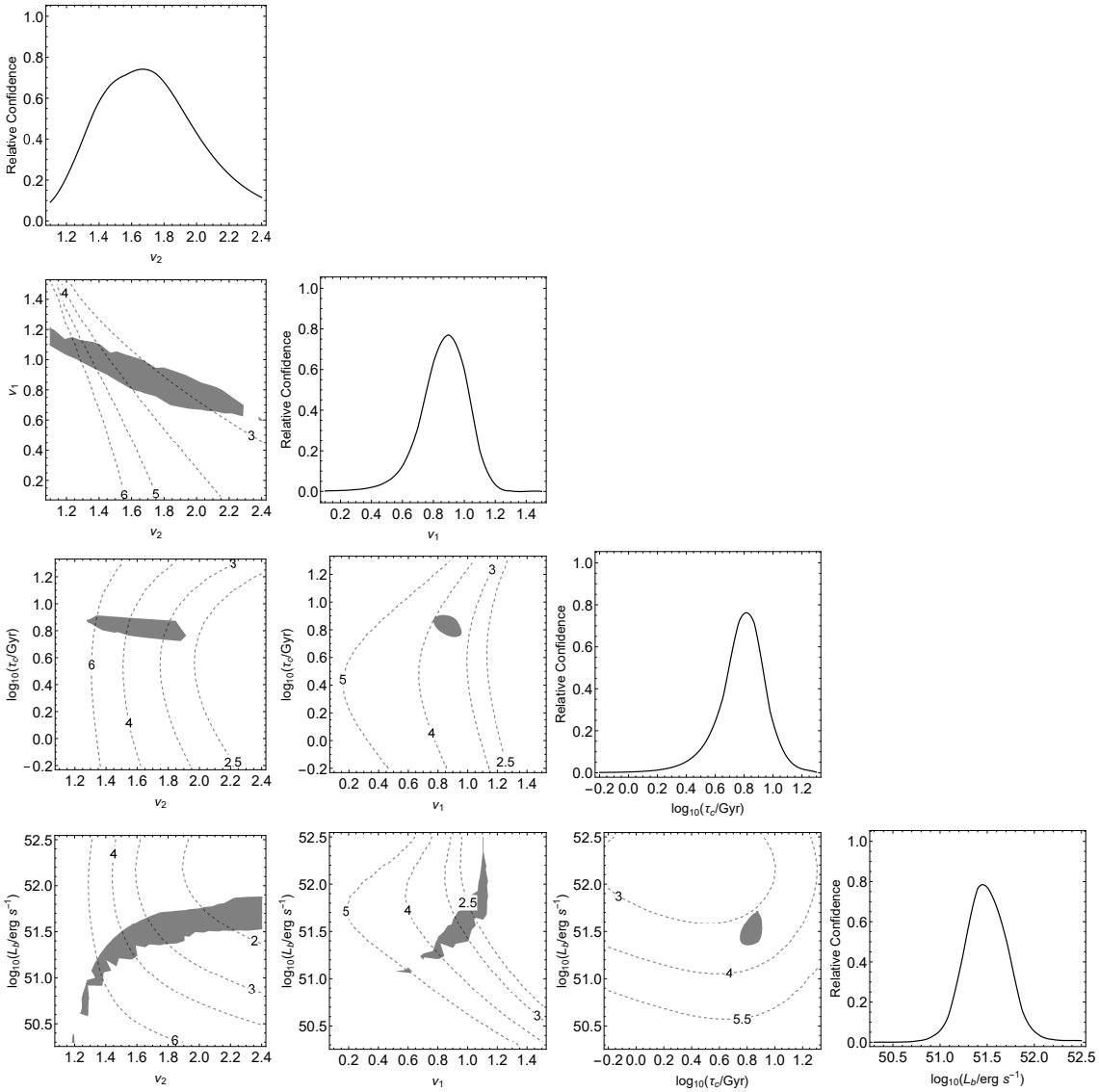

Fig. 3 Observational constraints on the model parameters. The $1-\sigma$ contour region is depicted as a shaded area in different panels. The dashed lines indicate the required local event rate of short GRBs as labeled by the numbers in units of $\mathrm{Gpc}^{-3}\mathrm{yr}^{-1}$.

Table 1 *Swift* Short GRBs with Measured Redshifts

GRBs	T_{90} s	S (10^{-7} erg cm^{-2})	$E_{\rm iso}$ (10^{50} erg)	$L_{\rm iso}$ (10^{51} erg s^{-1})	z
160624A	0.2	0.4	1.60	1.18	0.483
150423A	0.22	0.63	10.45	11.38	1.394
150120A	1.2	1.4	5.16	0.63	0.46
150101B	0.018	0.23	0.05	0.29	0.093
141212A	0.3	0.72	3.98	2.12	0.596
140903A	0.3	1.4	3.29	1.48	0.351
140622A	0.13	0.27	2.90	4.38	0.959
131004A	1.54	2.8	20.33	2.27	0.717
130603B	0.18	6.3	15.19	11.44	0.356
101219A	0.6	4.6	33.47	9.58	0.718
100724A	1.4	1.6	24.40	3.99	1.288
090510	0.3	3.4	33.85	21.47	0.903
090426	1.2	1.8	50.43	15.17	2.609
080905A	1	1.4	0.48	0.05	0.1218
071227	1.8	2.2	6.00	0.46	0.383
070724A	0.4	0.3	1.09	0.40	0.457
070429B	0.47	0.63	6.28	2.54	0.904
061217	0.21	0.42	3.72	3.24	0.827
061201	0.76	3.34	0.97	0.14	0.111
060801	0.49	0.8	10.52	4.57	1.13
060502B	0.131	0.4	0.66	0.65	0.287
051221A	1.4	11.5	55.78	6.16	0.547
050813	0.45	0.44	9.32	5.80	1.8
050509B	0.073	0.09	0.10	0.16	0.225
100625A	0.33	2.3	8.27	3.64	0.453
100206A	0.12	1.4	4.22	4.95	0.4068
100117A	0.3	0.93	9.49	6.07	0.92
090515	0.036	0.2	0.59	2.31	0.403
070729	0.9	1	8.46	1.69	0.8
051210	1.3	0.85	13.09	2.32	1.3
050724EE	96	9.98	13.71	0.02	0.2576
061006EE	130	14.2	48.30	0.05	0.4377
070714bEE	64	7.2	73.44	0.22	0.92
080123EE	115	5.7	23.64	0.03	0.495
091117A	0.4	3.5	0.77	0.21	0.096
100816aEE	2.9	20	170.71	10.62	0.8049

of a GRB jet can be empirically expressed by an exponential function as (e.g., Margutti et al. 2018)

$$E(\theta) \propto e^{-(\theta/\theta_{\rm c})^{\alpha}}, \tag{14}$$

where the characteristic angle $\theta_{\rm c}$ can be regarded as the opening angle of the core of a jet. The value of $\theta_{\rm c}$ should not be very different from the value of $\theta_{\rm j}$ estimated in the preceding section. In any case, such an angular energy distribution of GRB jets has been widely used to explain the multi-wavelength afterglows of GRB 170817A by assuming the line of sight deviates from the jet symmetry axis. Because of the drastic decrease in energy with increasing viewing angle θ, any off-axis observation of GRBs at relatively large distances would fail. Therefore, the top-hat assumption would be a very reasonable approximation. However, for sufficiently close sources such as GRB 170817A, the jet structure and the opportunity for off-axis observations become non-negligible. In this case, the number of detectable GRBs per year should be calculated by

$$\begin{aligned} N_{\rm obs} =& \frac{\Delta\Omega}{4\pi}\int_{z_1}^{z_2}\int_{L_1}^{L_2}\int_{0}^{\theta_{\rm max}} \dot{R}_{\rm SGRB}(z)\Phi(L_{\rm c}) \\ & \times \sin\theta {\rm d}\theta {\rm d}L\frac{{\rm d}V(z)}{1+z}, \end{aligned} \tag{15}$$

where the maximum angle $\theta_{\rm max}$ can be set at the position where the Lorentz factor of the jet becomes very close to unity. Here, it should be pointed out that the luminosity function derived in the preceding section actually only describes the distribution of the core luminosity of GRB jets, because of the on-axis assumption.

Table 2 Detection rates per year for different ranges of GRB luminosity and distance.

For *Swift* BAT

	<100 Mpc	100–200 Mpc	Sum
$10^{47}-10^{49}\,\mathrm{erg\,s^{-1}}$	1.5e–3	2.3e–3	3.8e–3
$10^{49}-10^{51}\,\mathrm{erg\,s^{-1}}$	8.0e–3	0.012	0.02
$10^{51}-10^{53}\,\mathrm{erg\,s^{-1}}$	3.2e–3	5.0e–3	8.2e–3
Sum	0.013	0.019	0.032

For GECAM

	<100 Mpc	100–200 Mpc	Sum
$10^{47}-10^{49}\,\mathrm{erg\,s^{-1}}$	0.015	0.023	0.038
$10^{49}-10^{51}\,\mathrm{erg\,s^{-1}}$	0.080	0.123	0.203
$10^{51}-10^{53}\,\mathrm{erg\,s^{-1}}$	0.032	0.049	0.081
Sum	0.127	0.195	0.322

Table 3 Parameters of Luminosity in Different Works

	ν_1	ν_2	$L_b(10^{51}\,\mathrm{erg\,s^{-1}})$
Guetta & Piran (2005)	0.6	2	2.2
Wanderman & Piran (2015)	0.5	1.5	4.6
Zhang & Wang (2018)	0.29	1.07	0.826
This paper	0.91	1.66	2.51

Therefore, in the above integration, the luminosity function should be calculated with a core luminosity that is determined by $L_{\rm c} = L\exp[(\theta/\theta_{\rm c})^{\alpha}]$. Finally, the obtained GRB numbers for different luminosity and distance ranges are listed in Table 2, where $\dot{R}_{\rm SGRB}(0) = 1540\,\mathrm{Gpc^{-3}\,yr^{-1}}$ is used and $\theta_{\rm c} \sim 3^{\circ}$ and $\alpha \sim 2$ are taken for consistency with the observational rate presented in Equation (13). The sensitivities and fields of view of *Swift* and the future Gravitational wave high-energy Electromagnetic Counterpart All-sky Monitor (GECAM) are taken as $P_{\rm th} = 5\times10^{-9}\,\mathrm{erg\,s^{-1}\,cm^{-2}}$, $\Delta\Omega/4\pi = 0.1$ and $2\times10^{-8}\,\mathrm{erg\,s^{-1}cm^{-2}}$, $\Delta\Omega/4\pi = 1.0$, respectively. Here, distances within the horizon ($D_{\rm LIGO,h} = 200\,\mathrm{Mpc}$) of Advanced LIGO are of interest. Within these distances, the number of detectable GRBs is insensitive to the telescope sensitivity but primarily dependent on their fields of view for the small difference in sum of the GRB numbers between *Swift* and GECAM.

5 SUMMARY AND DISCUSSION

With empirical expressions of observational selection effects given by Cao et al. (2011), we fit the redshift and luminosity distributions of 36 *Swift* short GRBs by assuming a broken-power-law luminosity function and connecting their event rates with CSFRs using power-law distributed delay times. As a result, the most-likely model parameters are constrained to be $\nu_1 = 0.91$, $\nu_2 = 1.66$, $L_b = 2.51\times10^{51}\,\mathrm{erg\,s^{-1}}$ and $\tau_c = 6.0\,\mathrm{Gyr}$. The parameters of the luminosity function have been compared with other works in Table 3. The corresponding local rate of short GRBs is found to be $\sim (3-4)\,\mathrm{Gpc^{-3}\,yr^{-1}}$. With these parameters, we predict the detectable numbers of short GRBs for different luminosity ranges and distance ranges within the horizon of Advanced LIGO, where the angular distribution of the emission energy of GRB jets is taken into account.

Acknowledgements This work is supported by the National Natural Science Foundation of China (Grant Nos. 11473008, 11822302 and 11833003) and the Fundamental Research Funds for the Central Universities (Grant No. CCNU18ZDPY06).

References

Abbott, B. P., Abbott, R., Abbott, T. D., et al. 2017, Physical Review Letters, 119, 161101
Belczynski, K., Kalogera, V., & Bulik, T. 2002, ApJ, 572, 407
Belczynski, K., Perna, R., Bulik, T., et al. 2006, ApJ, 648, 1110
Cao, X.-F., Yu, Y.-W., Cheng, K. S., & Zheng, X.-P. 2011, MNRAS, 416, 2174
Cao, X.-F., Yu, Y.-W., & Zhou, X. 2018, ApJ, 858, 89
Chornock, R., Berger, E., Levesque, E. M., et al. 2010, arXiv:1004.2262
Chruslinska, M., Belczynski, K., Klencki, J., & Benacquista, M. 2018, MNRAS, 474, 2937
Coward, D. M., Howell, E. J., Piran, T., et al. 2012, MNRAS, 425, 2668
Dietz, A. 2011, A&A, 529, A97
Eichler, D., Livio, M., Piran, T., & Schramm, D. N. 1989, Nature, 340, 126
Fiore, F., Guetta, D., Piranomonte, S., D'Elia, V., & Antonelli, L. A. 2007, A&A, 470, 515
Fong, W., Berger, E., Margutti, R., & Zauderer, B. A. 2015, ApJ, 815, 102
Gehrels, N., Sarazin, C. L., O'Brien, P. T., et al. 2005, Nature, 437, 851
Ghirlanda, G., Bernardini, M. G., Calderone, G., & D'Avanzo, P. 2015, Journal of High Energy Astrophysics, 7, 81
Ghirlanda, G., Salafia, O. S., Pescalli, A., et al. 2016, A&A, 594, A84
Gill, R., & Granot, J. 2018, MNRAS, 478, 4128
Goldstein, A., Veres, P., Burns, E., et al. 2017, ApJ, 848, L14
Greggio, L. 2005, A&A, 441, 1055
Guetta, D., & Piran, T. 2005, A&A, 435, 421
Guetta, D., & Piran, T. 2006, A&A, 453, 823
Guetta, D., & Stella, L. 2009, A&A, 498, 329
Hao, J.-M., & Yuan, Y.-F. 2013, A&A, 558, A22
Hjorth, J., Sollerman, J., Møller, P., et al. 2003, Nature, 423, 847
Hopkins, A. M., & Beacom, J. F. 2006, ApJ, 651, 142
Jin, Z.-P., Li, X., Wang, H., et al. 2018, ApJ, 857, 128

Kistler, M. D., Yüksel, H., Beacom, J. F., Hopkins, A. M., & Wyithe, J. S. B. 2009, ApJ, 705, L104
Kistler, M. D., Yüksel, H., Beacom, J. F., & Stanek, K. Z. 2008, ApJ, 673, L119
Kouveliotou, C., Meegan, C. A., Fishman, G. J., et al. 1993, ApJ, 413, L101
Lazzati, D., Perna, R., Morsony, B. J., et al. 2018, Physical Review Letters, 120, 241103
Maoz, D., Mannucci, F., & Brandt, T. D. 2012, MNRAS, 426, 3282
Margutti, R., Alexander, K. D., Xie, X., et al. 2018, ApJ, 856, L18
Mennekens, N., & Vanbeveren, D. 2016, A&A, 589, A64
Mennekens, N., Vanbeveren, D., De Greve, J. P., & De Donder, E. 2010, A&A, 515, A89
Mooley, K. P., Nakar, E., Hotokezaka, K., et al. 2018, Nature, 554, 207
Nakar, E., Gal-Yam, A., & Fox, D. B. 2006, ApJ, 650, 281
Narayan, R., Paczynski, B., & Piran, T. 1992, ApJ, 395, L83
Nava, L., Ghirlanda, G., Ghisellini, G., & Celotti, A. 2011, A&A, 530, A21
Paczynski, B. 1986, ApJ, 308, L43
Piran, T. 1992, ApJ, 389, L45
Portegies Zwart, S. F., & Yungelson, L. R. 1998, A&A, 332, 173
Ruiter, A. J., Belczynski, K., Sim, S. A., et al. 2011, MNRAS, 417, 408
Siellez, K., Boër, M., & Gendre, B. 2014, MNRAS, 437, 649
Stanek, K. Z., Matheson, T., Garnavich, P. M., et al. 2003, ApJ, 591, L17
Tan, W.-W., Fan, X.-L., & Wang, F. Y. 2018, MNRAS, 475, 1331
Totani, T., Morokuma, T., Oda, T., Doi, M., & Yasuda, N. 2008, PASJ, 60, 1327
Virgili, F. J., Zhang, B., O'Brien, P., & Troja, E. 2011, ApJ, 727, 109
Wanderman, D., & Piran, T. 2015, MNRAS, 448, 3026
Wang, F. Y. 2013, A&A, 556, A90
Yu, Y.-W., Cheng, K. S., Chu, M. C., & Yeung, S. 2012, J. Cosmol. Astropart. Phys., 7, 023
Zhang, B.-B., Zhang, B., Sun, H., et al. 2018, Nature Communications, 9, 447
Zhang, G. Q., & Wang, F. Y. 2018, ApJ, 852, 1